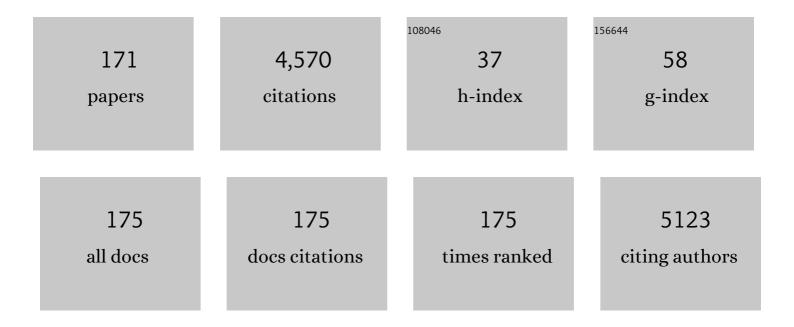
Shuo Li

List of Publications by Year in descending order

Source: https://exaly.com/author-pdf/3094115/publications.pdf Version: 2024-02-01



SHUOLI

#	Article	IF	CITATIONS
1	Few-Shot Learning for Deformable Medical Image Registration With Perception-Correspondence Decoupling and Reverse Teaching. IEEE Journal of Biomedical and Health Informatics, 2022, 26, 1177-1187.	3.9	15
2	Hematoma Expansion Context Guided Intracranial Hemorrhage Segmentation and Uncertainty Estimation. IEEE Journal of Biomedical and Health Informatics, 2022, 26, 1140-1151.	3.9	7
3	MVSGAN: Spatial-Aware Multi-View CMR Fusion for Accurate 3D Left Ventricular Myocardium Segmentation. IEEE Journal of Biomedical and Health Informatics, 2022, 26, 2264-2275.	3.9	3
4	Guest Editorial Generative Adversarial Networks in Biomedical Image Computing. IEEE Journal of Biomedical and Health Informatics, 2022, 26, 4-6.	3.9	0
5	Dihydropyrimidinone imidazoles as unique structural antibacterial agents for drug-resistant gram-negative pathogens. European Journal of Medicinal Chemistry, 2022, 232, 114188.	2.6	32
6	Discovery of unique thiazolidinone-conjugated coumarins as novel broad spectrum antibacterial agents. European Journal of Medicinal Chemistry, 2022, 232, 114192.	2.6	53
7	Regional Cardiac Motion Scoring With Multi-Scale Motion-Based Spatial Attention. IEEE Journal of Biomedical and Health Informatics, 2022, 26, 3116-3126.	3.9	0
8	Characterization of shape memory silane crossâ€linked lowâ€density polyethylene prepared by solidâ€phase grafting process. Journal of Applied Polymer Science, 2022, 139, .	1.3	1
9	MCAL: An Anatomical Knowledge Learning Model for Myocardial Segmentation in 2-D Echocardiography. IEEE Transactions on Ultrasonics, Ferroelectrics, and Frequency Control, 2022, 69, 1277-1287.	1.7	7
10	Novel metronidazole-derived three-component hybrids as promising broad-spectrum agents to combat oppressive bacterial resistance. Bioorganic Chemistry, 2022, 122, 105718.	2.0	23
11	Reasoning discriminative dictionary-embedded network for fully automatic vertebrae tumor diagnosis. Medical Image Analysis, 2022, 79, 102456.	7.0	6
12	Coumarin thiazoles as unique structural skeleton of potential antimicrobial agents. Bioorganic Chemistry, 2022, 124, 105855.	2.0	38
13	Estimating Functional Connectivity by Integration of Inherent Brain Function Activity Pattern Priors. IEEE/ACM Transactions on Computational Biology and Bioinformatics, 2021, 18, 2420-2430.	1.9	5
14	Automatic vertebrae recognition from arbitrary spine MRI images by a category-Consistent self-calibration detection framework. Medical Image Analysis, 2021, 67, 101826.	7.0	16
15	Sequential conditional reinforcement learning for simultaneous vertebral body detection and segmentation with modeling the spine anatomy. Medical Image Analysis, 2021, 67, 101861.	7.0	20
16	Unifying neural learning and symbolic reasoning for spinal medical report generation. Medical Image Analysis, 2021, 67, 101872.	7.0	22
17	Multitask Learning for Estimating Multitype Cardiac Indices in MRI and CT Based on Adversarial Reverse Mapping. IEEE Transactions on Neural Networks and Learning Systems, 2021, 32, 493-506.	7.2	29
18	Synthesis of gadolinium-enhanced liver tumors on nonenhanced liver MR images using pixel-level graph reinforcement learning. Medical Image Analysis, 2021, 69, 101976.	7.0	23

Shuo L

#	Article	IF	CITATIONS
19	OF-UMRN: Uncertainty-guided multitask regression network aided by optical flow for fully automated comprehensive analysis of carotid artery. Medical Image Analysis, 2021, 70, 101982.	7.0	4
20	Weakly-Supervised teacher-Student network for liver tumor segmentation from non-enhanced images. Medical Image Analysis, 2021, 70, 102005.	7.0	28
21	Estimating dual-energy CT imaging from single-energy CT data with material decomposition convolutional neural network. Medical Image Analysis, 2021, 70, 102001.	7.0	34
22	APRIL: Anatomical prior-guided reinforcement learning for accurate carotid lumen diameter and intima-media thickness measurement. Medical Image Analysis, 2021, 71, 102040.	7.0	12
23	Molecular design and preparation of 2-aminothiazole sulfanilamide oximes as membrane active antibacterial agents for drug resistant Acinetobacter baumannii. Bioorganic Chemistry, 2021, 113, 105039.	2.0	41
24	Quantifying Axial Spine Images Using Object-Specific Bi-Path Network. IEEE Journal of Biomedical and Health Informatics, 2021, 25, 2978-2987.	3.9	4
25	TSU-net: Two-stage multi-scale cascade and multi-field fusion U-net for right ventricular segmentation. Computerized Medical Imaging and Graphics, 2021, 93, 101971.	3.5	9
26	Thanka Mural Inpainting Based on Multi-Scale Adaptive Partial Convolution and Stroke-Like Mask. IEEE Transactions on Image Processing, 2021, 30, 3720-3733.	6.0	24
27	Crystal structure of the Cu(II) complex chlorido-(6-oxo-2-phenyl-1,6-dihydropyrimidine-4-carboxylato-k2 N,O)-(phenanthroline-k2) Tj ETQq1 1 0.784314 109-111.	4 rg₿Ţ_/Ové	erlo <u>c</u> k 10 Tf 50
28	Segmentation and quantification of infarction without contrast agents via spatiotemporal generative adversarial learning. Medical Image Analysis, 2020, 59, 101568.	7.0	40
29	Direct Cup-to-Disc Ratio Estimation for Glaucoma Screening via Semi-Supervised Learning. IEEE Journal of Biomedical and Health Informatics, 2020, 24, 1104-1113.	3.9	52
30	Multi-indices quantification of optic nerve head in fundus image via multitask collaborative learning. Medical Image Analysis, 2020, 60, 101593.	7.0	21
31	Commensal correlation network between segmentation and direct area estimation for bi-ventricle quantification. Medical Image Analysis, 2020, 59, 101591.	7.0	21
32	Ethylenic conjugated coumarin thiazolidinediones as new efficient antimicrobial modulators against clinical methicillin-resistant Staphylococcus aureus. Bioorganic Chemistry, 2020, 94, 103434.	2.0	63
33	Privileged Modality Distillation for Vessel Border Detection in Intracoronary Imaging. IEEE Transactions on Medical Imaging, 2020, 39, 1524-1534.	5.4	61
34	K-Net: Integrate Left Ventricle Segmentation and Direct Quantification of Paired Echo Sequence. IEEE Transactions on Medical Imaging, 2020, 39, 1690-1702.	5.4	41
35	Trustful Internet of Surveillance Things Based on Deeply Represented Visual Co-Saliency Detection. IEEE Internet of Things Journal, 2020, 7, 4092-4100.	5.5	32
36	Holistic multitask regression network for multiapplication shape regression segmentation. Medical Image Analysis, 2020, 65, 101783.	7.0	9

#	Article	IF	CITATIONS
37	Direct Quantification of Coronary Artery Stenosis Through Hierarchical Attentive Multi-View Learning. IEEE Transactions on Medical Imaging, 2020, 39, 4322-4334.	5.4	30
38	Image Projection Network: 3D to 2D Image Segmentation in OCTA Images. IEEE Transactions on Medical Imaging, 2020, 39, 3343-3354.	5.4	91
39	MB-FSGAN: Joint segmentation and quantification of kidney tumor on CT by the multi-branch feature sharing generative adversarial network. Medical Image Analysis, 2020, 64, 101721.	7.0	31
40	An integrated deep learning framework for joint segmentation of blood pool and myocardium. Medical Image Analysis, 2020, 62, 101685.	7.0	14
41	Multiple Axial Spine Indices Estimation via Dense Enhancing Network With Cross-Space Distance-Preserving Regularization. IEEE Journal of Biomedical and Health Informatics, 2020, 24, 3248-3257.	3.9	9
42	MMCL-Net: Spinal disease diagnosis in global mode using progressive multi-task joint learning. Neurocomputing, 2020, 399, 307-316.	3.5	18
43	Simultaneous left atrium anatomy and scar segmentations via deep learning in multiview information with attention. Future Generation Computer Systems, 2020, 107, 215-228.	4.9	73
44	Contrast agent-free synthesis and segmentation of ischemic heart disease images using progressive sequential causal GANs. Medical Image Analysis, 2020, 62, 101668.	7.0	39
45	SDAE-GAN: Enable high-dimensional pathological images in liver cancer survival prediction with a policy gradient based data augmentation method. Medical Image Analysis, 2020, 62, 101640.	7.0	7
46	Direct estimation of left ventricular ejection fraction via a cardiac cycle feature learning architecture. Computers in Biology and Medicine, 2020, 118, 103659.	3.9	8
47	Deep Atlas Network for Efficient 3D Left Ventricle Segmentation on Echocardiography. Medical Image Analysis, 2020, 61, 101638.	7.0	38
48	A far-red aza-crown ether fluorescent probe for selective G-quadruplex DNA targeting. Dyes and Pigments, 2020, 176, 108222.	2.0	7
49	MRLN: Multi-Task Relational Learning Network for MRI Vertebral Localization, Identification, and Segmentation. IEEE Journal of Biomedical and Health Informatics, 2020, 24, 2902-2911.	3.9	22
50	S ³ egANet: 3D Spinal Structures Segmentation via Adversarial Nets. IEEE Access, 2020, 8, 1892-1901.	2.6	9
51	Vessel Structure Extraction using Constrained Minimal Path Propagation. Artificial Intelligence in Medicine, 2020, 105, 101846.	3.8	3
52	Tripartite-GAN: Synthesizing liver contrast-enhanced MRI to improve tumor detection. Medical Image Analysis, 2020, 63, 101667.	7.0	54
53	EGDCL: An Adaptive Curriculum Learning Framework for Unbiased Glaucoma Diagnosis. Lecture Notes in Computer Science, 2020, , 190-205.	1.0	8
54	Dynamically constructed network with error correction for accurate ventricle volume estimation. Medical Image Analysis, 2020, 64, 101723.	7.0	9

Shuo L

#	Article	IF	CITATIONS
55	Deep Complementary Joint Model for Complex Scene Registration and Few-Shot Segmentation on Medical Images. Lecture Notes in Computer Science, 2020, , 770-786.	1.0	13
56	Automatic spondylolisthesis grading from MRIs across modalities using faster adversarial recognition network. Medical Image Analysis, 2019, 58, 101533.	7.0	23
57	Learning the implicit strain reconstruction in ultrasound elastography using privileged information. Medical Image Analysis, 2019, 58, 101534.	7.0	56
58	An Automated and Accurate Spine Curve Analysis System. IEEE Access, 2019, 7, 124596-124605.	2.6	34
59	Accurate automated Cobb angles estimation using multi-view extrapolation net. Medical Image Analysis, 2019, 58, 101542.	7.0	58
60	PV-LVNet: Direct left ventricle multitype indices estimation from 2D echocardiograms of paired apical views with deep neural networks. Medical Image Analysis, 2019, 58, 101554.	7.0	33
61	Cardiac-DeepIED: Automatic Pixel-Level Deep Segmentation for Cardiac Bi-Ventricle Using Improved End-to-End Encoder-Decoder Network. IEEE Journal of Translational Engineering in Health and Medicine, 2019, 7, 1-10.	2.2	33
62	Direct automated quantitative measurement of spine by cascade amplifier regression network with manifold regularization. Medical Image Analysis, 2019, 55, 103-115.	7.0	36
63	HHQ-4, a quinoline derivate, preferentially inhibits proliferation of glucose-deprived breast cancer cells as a GRP78 down-regulator. Toxicology and Applied Pharmacology, 2019, 373, 10-25.	1.3	9
64	Synthesis and Catalytic Activity of Activated Carbon Supported Sulfonated Cobalt Phthalocyanine in the Preparation of Dimethyl Disulfide. Applied Sciences (Switzerland), 2019, 9, 124.	1.3	8
65	Direct Segmentation-Based Full Quantification for Left Ventricle via Deep Multi-Task Regression Learning Network. IEEE Journal of Biomedical and Health Informatics, 2019, 23, 942-948.	3.9	27
66	Microalgal lipids production and nutrients recovery from landfill leachate using membrane photobioreactor. Bioresource Technology, 2019, 277, 18-26.	4.8	68
67	Multi-index Optic Disc Quantification via MultiTask Ensemble Learning. Lecture Notes in Computer Science, 2019, , 21-29.	1.0	2
68	Radiomics-guided GAN for Segmentation of Liver Tumor Without Contrast Agents. Lecture Notes in Computer Science, 2019, , 237-245.	1.0	12
69	Context-Aware Inductive Bias Learning for Vessel Border Detection in Multi-modal Intracoronary Imaging. Lecture Notes in Computer Science, 2019, , 776-784.	1.0	1
70	Automated Pathogenesis-Based Diagnosis of Lumbar Neural Foraminal Stenosis via Deep Multiscale Multitask Learning. Neuroinformatics, 2018, 16, 325-337.	1.5	25
71	Colorimetric detection of Cu2+ and UO22+ by mixed solvent effect. Dyes and Pigments, 2018, 152, 67-74.	2.0	10
72	Discovery of 2-aminothiazolyl berberine derivatives as effectively antibacterial agents toward clinically drug-resistant Gram-negative Acinetobacter baumanii. European Journal of Medicinal Chemistry, 2018, 146, 15-37.	2.6	83

Sнио l

#	Article	IF	CITATIONS
73	Multitarget Sparse Latent Regression. IEEE Transactions on Neural Networks and Learning Systems, 2018, 29, 1575-1586.	7.2	31
74	Multi-Target Regression via Robust Low-Rank Learning. IEEE Transactions on Pattern Analysis and Machine Intelligence, 2018, 40, 497-504.	9.7	101
75	Automated comprehensive Adolescent Idiopathic Scoliosis assessment using MVC-Net. Medical Image Analysis, 2018, 48, 1-11.	7.0	90
76	A far-red fluorescent probe for selective G-quadruplex DNA targeting. Tetrahedron Letters, 2018, 59, 3272-3278.	0.7	3
77	Spine-GAN: Semantic segmentation of multiple spinal structures. Medical Image Analysis, 2018, 50, 23-35.	7.0	125
78	Robust estimation of carotid artery wall motion using the elasticity-based state-space approach. Medical Image Analysis, 2017, 37, 1-21.	7.0	81
79	Design, synthesis and biological evaluation of novel Schiff base-bridged tetrahydroprotoberberine triazoles as a new type of potential antimicrobial agents. MedChemComm, 2017, 8, 907-916.	3.5	37
80	lsotope exchange reaction in tritium-contaminated vacuum pump oil: mechanism and HTO effect. RSC Advances, 2017, 7, 890-896.	1.7	3
81	Beat-to-Beat Blood Pressure and Two-dimensional (axial and radial) Motion of the Carotid Artery Wall: Physiological Evaluation of Arterial Stiffness. Scientific Reports, 2017, 7, 42254.	1.6	16
82	Direct spondylolisthesis identification and measurement in MR/CT using detectors trained by articulated parameterized spine model. , 2017, , .		6
83	Novel potentially antibacterial naphthalimide-derived metronidazoles: Design, synthesis, biological evaluation and supramolecular interactions with DNA, human serum albumin and topoisomerase II. Chinese Chemical Letters, 2017, 28, 1369-1374.	4.8	38
84	Preface. Computerized Medical Imaging and Graphics, 2017, 55, 1.	3.5	1
85	Unsupervised shape discovery using synchronized spectral networks. Pattern Recognition, 2017, 69, 39-51.	5.1	4
86	Direct and simultaneous estimation of cardiac four chamber volumes by multioutput sparse regression. Medical Image Analysis, 2017, 36, 184-196.	7.0	37
87	Unsupervised boundary delineation of spinal neural foramina using a multi-feature and adaptive spectral segmentation. Medical Image Analysis, 2017, 36, 22-40.	7.0	22
88	Flexible amine-functionalized triphenylamine derivative as a fluorescent "light-up―probe for G-quadruplex DNA. Dyes and Pigments, 2017, 136, 78-84.	2.0	21
89	Automated segmentation and area estimation of neural foramina with boundary regression model. Pattern Recognition, 2017, 63, 625-641.	5.1	17
90	Automated grading of lumbar disc degeneration via supervised distance metric learning. Proceedings of SPIE, 2017, , .	0.8	4

Shuo L

#	Article	IF	CITATIONS
91	DNA binding and cleavage properties of the Ce (III) complex of a diaza-crown ether. Progress in Reaction Kinetics and Mechanism, 2016, 41, 39-47.	1.1	6
92	DNA Cleavage and Condensation Activities of Mono- and Binuclear Hybrid Complexes and Regulation by Graphene Oxide. Molecules, 2016, 21, 920.	1.7	6
93	Automatic quantification of mammary glands on non-contrast x-ray CT by using a novel segmentation approach. Proceedings of SPIE, 2016, , .	0.8	1
94	Multi-modal vertebrae recognition using Transformed Deep Convolution Network. Computerized Medical Imaging and Graphics, 2016, 51, 11-19.	3.5	77
95	Exogenous Diethyl Aminoethyl Hexanoate, a Plant Growth Regulator, Highly Improved the Salinity Tolerance of Important Medicinal Plant Cassia obtusifolia L Journal of Plant Growth Regulation, 2016, 35, 330-344.	2.8	21
96	Spine labeling in axial magnetic resonance imaging via integral kernels. Computerized Medical Imaging and Graphics, 2016, 54, 27-34.	3.5	2
97	Quinazolinone azolyl ethanols: potential lead antimicrobial agents with dual action modes targeting methicillin-resistant <i>Staphylococcus aureus</i> DNA. Future Medicinal Chemistry, 2016, 8, 1927-1940.	1.1	51
98	A triphenylamine derivative as a naked-eye and light-up fluorescent probe for G-quadruplex DNA. Tetrahedron Letters, 2016, 57, 5042-5046.	0.7	8
99	Aggregation-induced emission active tetraphenylethene-based sensor for uranyl ion detection. Journal of Hazardous Materials, 2016, 318, 363-370.	6.5	54
100	Multi-task Shape Regression for Medical Image Segmentation. Lecture Notes in Computer Science, 2016, , 210-218.	1.0	2
101	Unmodified and positively charged gold nanoparticles for sensitive colorimetric detection of folate receptor via terminal protection of small molecule-linked ssDNA. Science China Chemistry, 2016, 59, 770-775.	4.2	6
102	Unsupervised Freeview Groupwise Cardiac Segmentation Using Synchronized Spectral Network. IEEE Transactions on Medical Imaging, 2016, 35, 2174-2188.	5.4	8
103	Descriptor Learning via Supervised Manifold Regularization for Multioutput Regression. IEEE Transactions on Neural Networks and Learning Systems, 2016, 28, 1-13.	7.2	10
104	Discovery of membrane active benzimidazole quinolones-based topoisomerase inhibitors as potential DNA-binding antimicrobial agents. European Journal of Medicinal Chemistry, 2016, 111, 160-182.	2.6	86
105	Detecting left ventricular impaired relaxation in cardiac MRI using moving mesh correspondences. Computer Methods and Programs in Biomedicine, 2016, 124, 58-66.	2.6	6
106	Fluorogenic Thorium Sensors Based on 2,6â€Pyridinedicarboxylic Acid‣ubstituted Tetraphenylethenes with Aggregationâ€Induced Emission Characteristics. Chemistry - an Asian Journal, 2016, 11, 49-53.	1.7	32
107	Polyethylenimine analogs for improved gene delivery: effect of the type of amino groups. RSC Advances, 2016, 6, 5391-5400.	1.7	8
108	Development of the aza-crown ether metal complexes as artificial hydrolase. Journal of Inorganic Biochemistry, 2016, 154, 89-102.	1.5	29

#	Article	IF	CITATIONS
109	Multi-scale deep networks and regression forests for direct bi-ventricular volume estimation. Medical Image Analysis, 2016, 30, 120-129.	7.0	95
110	Automated Diagnosis of Neural Foraminal Stenosis Using Synchronized Superpixels Representation. Lecture Notes in Computer Science, 2016, , 335-343.	1.0	2
111	Carotid Artery Wall Motion Estimated from Ultrasound Imaging Sequences Using a Nonlinear State Space Approach. Lecture Notes in Computer Science, 2016, , 98-106.	1.0	1
112	Localization and Segmentation of 3D Intervertebral Discs from MR Images via a Learning Based Method: A Validation Framework. Lecture Notes in Computer Science, 2016, , 141-149.	1.0	0
113	Supervised descriptor learning for multi-output regression. , 2015, , .		21
114	Regression Segmentation for <formula formulatype="inline"><tex Notation="TeX">\$M^{3}\$</tex </formula> Spinal Images. IEEE Transactions on Medical Imaging, 2015, 34, 1640-1648.	5.4	48
115	Multi-Modality Vertebra Recognition in Arbitrary Views Using 3D Deformable Hierarchical Model. IEEE Transactions on Medical Imaging, 2015, 34, 1676-1693.	5.4	60
116	Reversible PEGylation and Schiff-base linked imidazole modification of polylysine for high-performance gene delivery. Journal of Materials Chemistry B, 2015, 3, 1507-1517.	2.9	20
117	Theoretical investigation of the mechanism of tritiated methane dehydrogenation reaction using nickel-based catalysts. Fusion Engineering and Design, 2015, 95, 91-98.	1.0	2
118	Direct and Simultaneous Four-Chamber Volume Estimation by Multi-Output Regression. Lecture Notes in Computer Science, 2015, , 669-676.	1.0	24
119	Incremental learning for <mml:math <br="" xmlns:mml="http://www.w3.org/1998/Math/MathML">altimg="si17.gif" display="inline" overflow="scroll"> <mml:mi>ν2 </mml:mi> </mml:math> -Support Vector Regression. Neural Networks, 2015, 67, 140-150.	3.3	473
120	Distribution Matching with the Bhattacharyya Similarity: A Bound Optimization Framework. IEEE Transactions on Pattern Analysis and Machine Intelligence, 2015, 37, 1777-1791.	9.7	23
121	Medical image computing in diagnosis and intervention of spinal diseases. Computerized Medical Imaging and Graphics, 2015, 45, 99-101.	3.5	5
122	A triphenylamine-based colorimetric and fluorescent probe with donor–bridge–acceptor structure for detection of G-quadruplex DNA. Bioorganic and Medicinal Chemistry Letters, 2015, 25, 5672-5676.	1.0	18
123	Unsupervised Free-View Groupwise Segmentation for M3 Cardiac Images Using Synchronized Spectral Network. Lecture Notes in Computer Science, 2015, , 280-288.	1.0	2
124	Synthesis, Characterisation and Molecular Recognition of Novel Zn(II) Macrocyclic Complexes with Imidazole or Benzimidazole Pendants. Journal of Chemical Research, 2014, 38, 102-107.	0.6	1
125	Direct Estimation of Cardiac Bi-ventricular Volumes with Regression Forests. Lecture Notes in Computer Science, 2014, 17, 586-593.	1.0	41
126	Detecting left ventricular impaired relaxation using MR imaging. , 2014, , .		0

#	Article	IF	CITATIONS
127	Direct Estimation of Cardiac Biventricular Volumes With an Adapted Bayesian Formulation. IEEE Transactions on Biomedical Engineering, 2014, 61, 1251-1260.	2.5	54
128	Activity of a New Metallomicelle Catalytic System on the Hydrolysis of bis(4-nitrophenyl) Phosphate Ester. Journal of Dispersion Science and Technology, 2014, 35, 411-417.	1.3	7
129	Regional Assessment of Cardiac Left Ventricular Myocardial Function via MRI Statistical Features. IEEE Transactions on Medical Imaging, 2014, 33, 481-494.	5.4	71
130	The synthesis and activities of novel mononuclear or dinuclear cyclen complexes bearing azole pendants as antibacterial and antifungal agents. European Journal of Medicinal Chemistry, 2014, 84, 677-686.	2.6	27
131	Regional heart motion abnormality detection: An information theoretic approach. Medical Image Analysis, 2013, 17, 311-324.	7.0	35
132	Intervertebral disc segmentation in MR images using anisotropic oriented flux. Medical Image Analysis, 2013, 17, 43-61.	7.0	59
133	Gradient Competition Anisotropy for Centerline Extraction and Segmentation of Spinal Cords. Lecture Notes in Computer Science, 2013, 23, 49-61.	1.0	7
134	Pixel level image fusion for medical imaging: an energy minimizing approach. Proceedings of SPIE, 2012, , .	0.8	4
135	Estimation of the Cardiac Ejection Fraction from image statistics. , 2012, , .		0
136	A Convex Max-Flow Approach to Distribution-Based Figure-Ground Separation. SIAM Journal on Imaging Sciences, 2012, 5, 1333-1354.	1.3	24
137	Biodegradable cyclen-based linear and cross-linked polymers as non-viral gene vectors. Bioorganic and Medicinal Chemistry, 2012, 20, 1380-1387.	1.4	16
138	Max-flow segmentation of the left ventricle by recovering subject-specific distributions via a bound of the Bhattacharyya measure. Medical Image Analysis, 2012, 16, 87-100.	7.0	72
139	Global Assessment of Cardiac Function Using Image Statistics in MRI. Lecture Notes in Computer Science, 2012, 15, 535-543.	1.0	16
140	Dilated Divergence Based Scale-Space Representation for Curve Analysis. Lecture Notes in Computer Science, 2012, , 557-571.	1.0	2
141	Regional Heart Motion Abnormality Detection via Multiview Fusion. Lecture Notes in Computer Science, 2012, 15, 527-534.	1.0	5
142	Biodegradable cross-linked poly(amino alcohol esters) based on LMW PEI for gene delivery. Molecular BioSystems, 2011, 7, 1254.	2.9	25
143	Graph Cuts with Invariant Object-Interaction Priors: Application to Intervertebral Disc Segmentation. Lecture Notes in Computer Science, 2011, 22, 221-232.	1.0	44
144	Variational level-set segmentation and tracking of left ventricle using field prior. Proceedings of SPIE, 2011, , .	0.8	0

#	Article	IF	CITATIONS
145	A neural network learned information measures for heart motion abnormality detection. , 2011, , .		0
146	A Convex Max-Flow Segmentation of LV Using Subject-Specific Distributions on Cardiac MRI. Lecture Notes in Computer Science, 2011, 22, 171-183.	1.0	3
147	Assessment of Regional Myocardial Function via Statistical Features in MR Images. Lecture Notes in Computer Science, 2011, 14, 107-114.	1.0	7
148	Tracking Endocardial Motion Via Multiple Model Filtering. IEEE Transactions on Biomedical Engineering, 2010, 57, 2001-2010.	2.5	18
149	Detection of Left Ventricular Motion Abnormality Via Information Measures and Bayesian Filtering. IEEE Transactions on Information Technology in Biomedicine, 2010, 14, 1106-1113.	3.6	17
150	Finding image distributions on active curves. , 2010, , .		1
151	Graph cut segmentation with a global constraint: Recovering region distribution via a bound of the Bhattacharyya measure. , 2010, , .		27
152	Regional Heart Motion Abnormality Detection via Information Measures and Unscented Kalman Filtering. Lecture Notes in Computer Science, 2010, 13, 409-417.	1.0	11
153	Tracking Endocardial Boundary and Motion via Graph Cut Distribution Matching and Multiple Model Filtering. Lecture Notes in Computer Science, 2010, , 172-182.	1.0	0
154	Embedding Overlap Priors in Variational Left Ventricle Tracking. IEEE Transactions on Medical Imaging, 2009, 28, 1902-1913.	5.4	66
155	A Statistical Overlap Prior for Variational Image Segmentation. International Journal of Computer Vision, 2009, 85, 115-132.	10.9	28
156	Myocardium tracking via matching distributions. International Journal of Computer Assisted Radiology and Surgery, 2009, 4, 37-44.	1.7	4
157	Level Set Image Segmentation with a Statistical Overlap Constraint. Lecture Notes in Computer Science, 2009, 21, 589-601.	1.0	4
158	Left Ventricle Segmentation via Graph Cut Distribution Matching. Lecture Notes in Computer Science, 2009, 12, 901-909.	1.0	32
159	Heart Motion Abnormality Detection via an Information Measure and Bayesian Filtering. Lecture Notes in Computer Science, 2009, 12, 373-380.	1.0	4
160	Tracking distributions with an overlap prior. , 2008, , .		6
161	Area prior constrained level set evolution for medical image segmentation. , 2008, , .		1
162	Left Ventricle Tracking Using Overlap Priors. Lecture Notes in Computer Science, 2008, 11, 1025-1033.	1.0	17

#	Article	IF	CITATIONS
163	Computer aided root lesion detection using level set and complex wavelets. , 2007, , .		0
164	Semi-automatic computer aided lesion detection in dental X-rays using variational level set. Pattern Recognition, 2007, 40, 2861-2873.	5.1	63
165	Motion learning-based framework for unarticulated shape animation. Visual Computer, 2007, 23, 753-761.	2.5	2
166	Automatic clinical image segmentation using pathological modeling, PCA and SVM. Engineering Applications of Artificial Intelligence, 2006, 19, 403-410.	4.3	43
167	An automatic variational level set segmentation framework for computer aided dental X-rays analysis in clinical environments. Computerized Medical Imaging and Graphics, 2006, 30, 65-74.	3.5	43
168	Fast and Robust Clinical Triple-Region Image Segmentation Using One Level Set Function. Lecture Notes in Computer Science, 2006, 9, 766-773.	1.0	5
169	A level set segmentation for computer-aided dental x-ray analysis. , 2005, , .		3
170	Automatic Clinical Image Segmentation Using Pathological Modelling, PCA and SVM. Lecture Notes in Computer Science, 2005, , 314-324.	1.0	4
171	Toward Automatic Computer Aided Dental X-ray Analysis Using Level Set Method. Lecture Notes in Computer Science, 2005, 8, 670-678.	1.0	6